Journal of
Synchrotron
Radiation

ISSN 1600-5775

Received 27 May 2014
Accepted 11 September 2014

X-ray focusing scheme with continuously variable lens

Bernhard W. Adams[a]* and Christoph Rose-Petruck[b]

[a]Argonne National Laboratory, 9700 South Cass Avenue, Argonne, IL 60439, USA, and [b]Brown University, Providence, RI 02912, USA. *E-mail: adams@aps.anl.gov

A novel hybrid X-ray focusing scheme was developed for operation of the X-ray streak camera at the Advanced Photon Source: an X-ray lens focuses vertically from a long distance of 16 m and produces an extended focus that has a small footprint on an inexpensive sagittal mirror. A patented method is used to continuously adjust the focal length of the lens and compensate for chromatic dispersion in energy scans.

Keywords: X-ray focusing; continuously variable focal length.

1. Introduction

Making the best possible use of X-rays at a synchrotron beamline often requires focusing in a specific way. For example, a short focal length allows a tight focus, but only within a short Rayleigh length, and it also broadens rocking curves in X-ray diffraction experiments. In most cases there is an intrinsic anisotropy in the experiment, such as due to a particular plane of diffraction, and the optimization of the focusing properties needs to be done separately in two transverse directions. The commonly used X-ray focusing elements, namely compound refractive lenses, mirrors and Fresnel zone plates, each have specific strengths and problems, so their use has to be matched to the requirements: lenses can accept large beams at relatively low cost, but exhibit chromatic dispersion. Zone plates can achieve the tightest focal spot sizes down to about 20 nm, but they also exhibit chromatic dispersion, and they are also very delicate. Furthermore, zone plates are not available for long focal lengths, such as those required here (see below). Mirrors are dispersionless but, due to the small incidence angle, need to be very large to intercept a large beam. Both the dispersion of lenses and zone plates, and the wavelength dependence of the critical angle of total reflection in mirrors are used to suppress shorter-wavelength X-ray harmonics in spectroscopic applications. Unlike lenses or zone plates, a mirror changes the direction of a beam axis. It is therefore very impractical to use a single focusing mirror for a long focal length.

A lens with a spherical thickness profile (or circular profile in the case of a one-dimensionally focusing lens) exhibits spherical aberration. This is a major problem for imaging applications, and therefore parabolic X-ray lenses were developed for both two-dimensional (Lengeler *et al.*, 1999) and one-dimensional focusing (Lengeler, 2010). However, some aberrations can be tolerated in applications where the goal is only to concentrate X-ray flux into a small aperture, such as here the focal spot of a laser on the sample, as well as the entrance slit of the streak camera about 70 cm downstream from it. In such an application, aberrations just lead to some minor loss of X-ray flux that is not entering the aperture. It may then be more economical to use spherical lenses for two-dimensional focusing, or circular-cross-section cylinders for one-dimensional focusing. Especially for the latter, the cost of simply drilling a hole into a piece of matter is considerably less than shaping a parabolic profile.

In most applications it is necessary to adjust the focus of an optical element. This is especially important for dispersive elements (refractive lens and zone plate) when the X-ray wavelength is changed in spectroscopic applications. At constant wavelength, the focal length of a zone plate is fixed, and the only way the focus can be adjusted is by moving the zone plate. The focal length of a mirror can be adjusted by bending (such as in the Kirkpatrick–Baez system) or by change of the incidence angle in sagittal mirrors. With compound lenses, two ways of focal-length adjustment are commonly used, namely change of the number N of component lenses, or by changing the angular setting of a sawtooth lens (Arms *et al.*, 2002; Ribbing *et al.*, 2003; Shastri *et al.*, 2007). An adjustment of the number of lenses can be made in discrete steps by insertion and removal of lens elements [the 'transfocator' developed at the European Synchrotron-Radiation Facility (Vaughan *et al.*, 2011; Zozulya *et al.*, 2012)], or by shaping the compound lens as a wedge, so that a lateral translation brings a variable number of holes into the beam (Khounsary *et al.*, 2002). Here, a novel way of continuously varying the effective number of focusing elements is presented (Adams & Chollet, 2013).

Operation of the X-ray streak camera at sector 7 (Dufresne *et al.*, 2010) of the Advanced Photon Source (APS) requires focusing optics that, at the sample location, provide a 20–50 μm focus in both the horizontal (h) and vertical (v) directions, as well as 20–50 μm (h) by 500 μm (v) on the entrance slit of the streak camera about 50 cm further downstream. The small vertical focus in two points separated by 50 cm requires

a long focal length, and the requirement to focus on the sample but spread the beam horizontally on the entrance slit requires a short focal length. Furthermore, diffraction experiments require preservation of beam collimation within the diffraction plane, and thus also a long focal length. Finally, spectroscopic experiments require suppression of X-ray harmonics. In combined laser–X-ray experiments it is critical to maintain spatial overlap of the focal spots. This is accomplished here by a precision slit with integrated beam-position monitor function and a modified version of the monochromator stabilizer (MOSTAB) (Krolzig *et al.*, 1984). With these properties and constraints in mind, a hybrid lens/mirror focusing system was designed and tested in combination with a high-resolution focal-spot stabilizer.

2. Specifics of the focusing requirements

Although a continuously variable X-ray lens will be useful in many different beamline applications, it shall now be discussed specifically in view of the operation of the hard-X-ray streak camera of the APS (Chollet *et al.*, 2011). These detectors (Liu *et al.*, 2003; Feng *et al.*, 2007*a*,*b*) can achieve a picosecond time resolution, which is faster than the natural bunch duration of a synchrotron storage ring. They are used for the study of rapid structural and electronic changes in samples, such as, for example, the role of a solvent in ligand photodetachment of $Fe(CO)_5$ (Ahr *et al.*, 2011). The operating principle of rapidly deflecting an electron beam from a photocathode to generate a time-correlated image (the 'streak') requires that the sensitive area be narrow in the streak direction. The X-rays must be focused at least one-dimensionally into this aperture, as well as into a laser–X-ray interaction spot at some distance from the photocathode. With respect to the other transverse direction, an X-ray focus needs to lie within the laser focus, but the X-rays may spread out on their way to the streak camera to cover some portion of the entrance slit width. Such a horizontal spreading may even be desirable to reduce localized radiation-induced degradation of the photocathode.

In the present application the X-ray beam from the monochromator is about 500 µm high, the X-ray beam size has to be less than 50 µm at the sample and 25 µm at the photocathode, and the sample is about 50 cm upstream of the photocathode. By looking at the divergences in terms of geometric optics, the focusing optic then has to be at least 3.2 m upstream of the sample to meet these requirements. Wave optics, on the other hand, places an upper limit on the focal length as follows: with a vertical coherence length of 50 µm, there are ten transverse modes in the vertical direction of a 500 µm beam. Then, to obtain a vertical beam size of 25 µm, the Gaussian waist w_0 has to be 1/10 of that size (the number of transverse modes). The Rayleigh range for this focus at a wavelength of 1.5 Å is $z_r = \pi w_0^2/\lambda = 0.131$ m. Then, with the Gaussian beam-diameter formula $w = w_0(1 + z^2/z_r^2)$, one transverse mode expands to less than 10 µm within the distance between sample and photocathode, and to a size of 500 µm at a distance of $200z_r = 26.2$ m. This latter number gives the maximum distance for the optic to focus a 500 µm beam.

In diffraction experiments, another aspect also comes into play: focusing necessarily introduces an angular divergence that broadens the rocking curves of samples. For example, even at the maximum focal distance of 26 m for a 500 µm beam, the geometric optical divergence of 19 µrad exceeds the rocking width of Si (111) at 8 keV. High-resolution diffraction experiments with focusing will therefore require the use of another crystal that is dispersion-matched to the sample to act as an angular filter. Nonetheless, in order to minimize the losses in this filtering, the focusing element should be placed as far upstream of the sample as other constraints allow.

In the present case, the beamline layout permits a 'far' placement of the vertically focusing optic at distances between about 10 and 16 m from the sample. This optic has to be a lens because zone plates are not available for that distance, and a mirror would deflect the beam far outside the beam transport path. The long focal length requires a lens with very large holes for a large radius of curvature, or a lens with very few holes. Large holes with thin walls would suffer from mechanical stability problems, so the choice was made to use a lens made of Be metal with two holes of 1 mm diameter, *i.e.* three walls. The usual method of adjusting the focal length by changing the number of holes obviously would yield very coarse steps, and therefore, a method of continuously varying the effective number of holes was employed. This will be the main topic of this paper. As discussed above, the entrance aperture of the streak camera is 3 mm wide, so no extended focus is required for the horizontal direction. Furthermore, with a horizontal source size of 280 µm (APS, 2013), a demagnification of at least a factor of 11 is required to achieve a horizontal focal-spot size of 25 µm. Therefore, the horizontally focusing optic can be no more than 1/11 of the 51.5 m distance of the sample from the source. Here, the beamline layout permitted a location 1.0 m from the sample. In addition to focusing, the optic should also suppress harmonics. This focusing task can be done by a compound-refractive lens or by a sagittal mirror. Both provide the additional benefit of suppressing harmonic energy photons in the beam, which is of utmost importance for spectroscopy. However, the lens can do so only if a small aperture is placed near the focus because, otherwise, the less-focused harmonic content would still be overlaid on the image, or, here, on the streak-camera entrance slit. Even so, the harmonic suppression from a lens is roughly proportional to the ratio of the focal spots at the respective energies, which amounts, for a 500 µm beam and a 25 µm focus, to a factor of about 20. A mirror with the present parameters [7.1 keV, incidence at 0.115° (see below), specified r.m.s. roughness of 5 Å] will achieve the same factor of 100 in the suppression of the third harmonic of 7.1 keV. A lens at the short focal length of 1 m and holes of 1 mm-diameter would need 37 holes to focus at 7.1 keV [see equation (2) below]. This would severely restrict the continuous focal adjustment as described below, but a stepwise change of the number of holes would be quite reasonable. With the vertically focused X-rays, a rather small wedge angle of a few degrees would, in fact, be

sufficient for this stepwise adjustment in the way of Khounsary *et al.* (2002). Likewise, a sagittal mirror benefits from the small vertical size because its footprint on the mirror is less than 20 mm (see below). This greatly reduces the cost of the mirror and its enclosure and actuators. Given these considerations, the choice fell here to using a focusing mirror, but the balance might well tip the other way in other applications.

3. X-ray lens with variable focal length

The X-ray refractive index n of a material is commonly written as $n = 1 - \delta + i\beta$ with the refractive decrement δ,

$$\delta = r_e \lambda^2 \rho / 2\pi, \tag{1}$$

where $r_e = 2.82 \times 10^{-15}$ m is the classical electron radius, λ is the X-ray wavelength, and ρ is the electron density of the material. In beryllium, the lens material commonly used for its low absorption, $\rho = 4.94 \times 10^{29}$ m^{-3}. The term β represents absorption. In light elements, such as Be, it is rather small ($\sim 3.8 \times 10^{-9}$ in Be at 7.1 keV), and will therefore be ignored, here.

X-rays traversing a length d of matter will acquire a phase advance of $d\delta$ relative to the same distance in vacuum. A single plano-concave (PCV) lens with a radius of curvature (ROC) of R has the shape $d(x) = R[1 - (1 - x^2/R^2)^{1/2}] \simeq x^2/2R$, where x is the transverse beam coordinate (see Fig. 1). Then, $\delta d \simeq x^2/(2R/\delta)$, and the lens will impart a curvature on the wavefronts passing through it with a ROC of $r = R/\delta$, and r is the focal length of the single PCV lens. For a detailed theory of the wave optics of X-ray lenses, see Kohn (2003).

Because δ is so small, the focal length is much larger than the radius of curvature, and the thin-lens approximation is valid even if several holes are lined up in a compound refractive lens (CRL) to obtain a stronger focusing power. A CRL with N holes, *i.e.* $\mathcal{N} = 2N$ curved surfaces, can then be treated as $2N$ plano-convex surfaces with each contributing an x-dependent phase advance on a plane wave, leading to a focal length that is $2N$ times shorter than that of a single PCV lens to yield the well known formula for X-ray lenses,

$$f = R/2N\delta. \tag{2}$$

For values of x that are not small compared with R, deviations of a circle from the parabolic shape $d \simeq x^2/R$ lead to cylindrical aberrations. However, given a parabolic surface with $1/2R$, the coefficient of x^2, the expression $r = R/\delta$ is a good approximation of the ROC and the focal length because, certainly, $x \ll r$.

With a lens in a given location, its focal length needs to be adjusted to place the focus onto a sample (also in a fixed location). Due to the wavelength dispersion of δ in equation (1), this adjustment is strongly wavelength-dependent. A commonly used method for adjusting the focal length is to vary the number of holes, for example by shaping the lens body like a wedge (Khounsary *et al.*, 2002), and translating it to bring a variable number of holes into the beam. This method is not useful here because the small number of holes of a long focal lens would make for rather coarse steps in the focal-length adjustment.

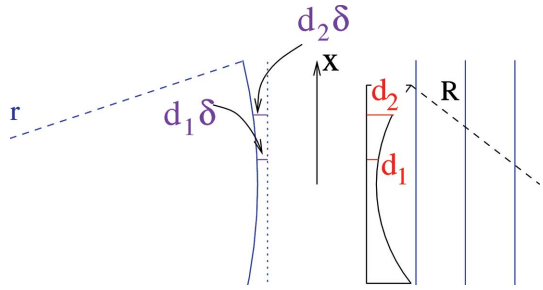

Figure 1
A curved surface with ROC of R will impart a curvature on incident plane waves whose ROC is $r = R/\delta$ (see text).

There is, however, a way (Adams & Chollet, 2013) to continuously vary the effective number of holes of a lens, as shown in Fig. 2. To explain this, we first define the laboratory coordinates (x, y, z) according to the convention used at the APS with x in the outboard direction from the storage ring, y going up, and z along the X-ray beam. Then, the lens coordinates (u, v, w) are: u along the cylinder bore, and v, w perpendicular to u and each other, and aligned along the cut surfaces of the lens block, as shown in Fig. 2. By rotating the lens by an angle χ about the v axis, the same scaling factor

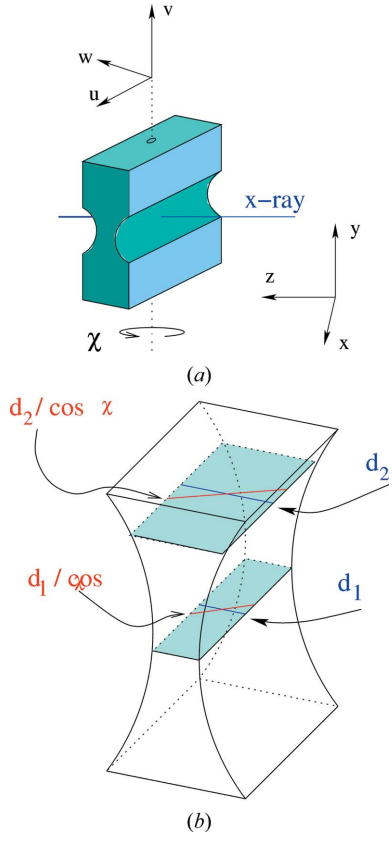

Figure 2
Top: rotation of a lens about the χ axis. Shown is a wall between two holes, corresponding to two of the PCV lenses shown in Fig. 1. Bottom: at $\chi = 0$, rays traversing the wall travel lengths d_1, d_2 on- and off-axis, respectively. After rotation, both paths are scaled up by the same factor, $1/\cos\chi$. This changes the number N of walls to the equivalent of $N/\cos\chi$ walls.

$1/\cos\chi$ is introduced for the amount of material traversed by each ray. In light of the above wave-optical consideration of an X-ray lens, this rotation has exactly the same effect as an increase of the number $\mathcal{N}$ of curved surfaces of holes by a factor of $1/\cos\chi$. However, unlike the case of real holes, this factor need not be an integer. Furthermore, the character of the lens surface is preserved, *i.e.* a cylindrical curvature stays cylindrical and a parabola remains parabolic.

4. Short sagittally focusing mirror

At its location close to the focus of the lens, the mirror intercepts an X-ray beam that is only about 40 µm high. Therefore, the footprint on the mirror is much shorter than it would be for an unfocused beam, and a rather inexpensive short sagittal mirror can be used. Here, the sagittal mirror is 150 mm long, which is far longer than actually required (see below), and is only due to the availablility of precision-polished glass. The mirror has a cylindrical surface with a radius of curvature $r = 4$ mm, and it is set to an incidence angle of $\Theta \simeq 0.115^\circ$ for focusing at 1 m (see §7). We proceed to calculate the footprint within the plane defined by the center of the lens line focus, and the X-ray propagation direction, as shown in Fig. 3: first, we define coordinates x', z' within the plane. Then, given a value $x' = \xi$, we calculate η shown in Fig. 3, which is related to $\zeta = \eta/\tan\Theta$. The upper right-hand figure shows $\eta = r - (r^2 - \xi^2)^{1/2} \simeq r - r(1 - \xi^2/2r^2) = \xi^2/2r$, and thus

$$\zeta \simeq \xi^2/(2r\tan\Theta). \qquad (3)$$

For each ξ, the incident beam height h is projected onto the mirror surface, leading to a local footprint of $\ell = h/\tan\Theta$ at each ξ of the parabola. For a 500 µm-wide beam, *i.e.* $\xi = -250$ µm to +250 µm, $r = 4$ mm, and $\Theta = 0.115^\circ$ (the angle of optimal focusing in the present application, see §7), the parabola takes values of 0–3.9 mm, and the local footprint with a vertical focus of 35 µm is $\ell = 17.5$ mm, as shown in Fig. 4. Therefore, the mirror could actually be considerably shorter than 150 mm. The first test of the focusing concept was, in fact, performed with a concave 12.5 mm-long fused-silica cylindrical lens. However, the surface finish, although sufficient for laser optics, led to considerable diffuse scattering of the X-rays, and a precision-polished mirror with an r.m.s. surface roughness of 5 Å had to be procured (Insync, 2011).

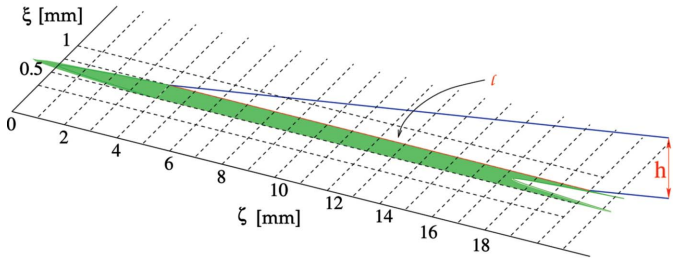

Figure 4
Footprint of an incident beam on the sagittal mirror within the incidence plane. The beam has a height $h = 35$ µm, which is projected onto a length $\ell = 17.5$ mm at an incidence angle $\Theta = 0.115^\circ$. The parabolic shape of the conic intersection adds another 4 mm to that.

5. Beam stabilizer

As is common practice, the double-diamond-crystal X-ray monochromator at the 7-ID beamline of the APS uses a piezoelectric actuator for fine-tuning the angular setting of the second crystal. This angular setting affects both the overlap of the two crystal reflectivity curves and the pointing of the X-rays traveling down the beamline. Both change over time due to electron-beam steering, mechanical strain on the monochromator during scans of the photon energy, changes in the heat load on the monochromator due to undulator-gap changes, *etc*. A slit consisting of two offset vertically movable steel rods (see Fig. 5) placed about 20 cm upstream of the sample is adjusted to ensure that the only X-rays that reach the streak camera are those that go through the laser focus in the sample. This slit doubles as a beam-position monitor (BPM) that is used by feedback electronics to control the piezo such that the focus remains within the slit. This feedback system operates on the principle of the MOSTAB (Krolzig *et al.*, 1984) and will be described in detail elsewhere.

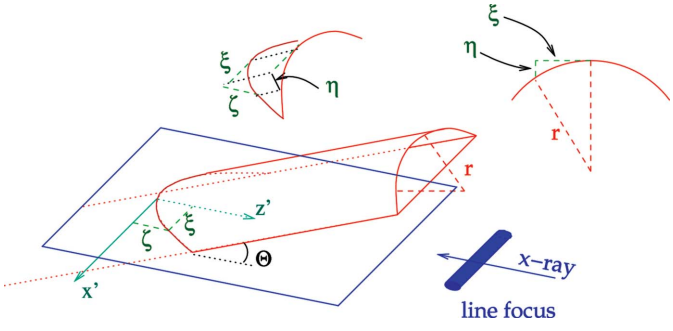

Figure 3
Intersection of the cylindrical mirror surface with the incidence plane given by the incident X-rays (swept out by the line focus as it propagates). The intersection curve is a parabola (a conical section), which is calculated in the text.

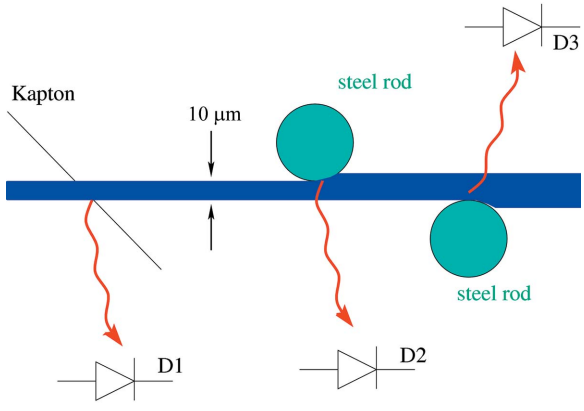

Figure 5
Schematic of the slit/BPM system. Two steel rods form a slit for the X-rays, and scatter/fluorescence from them is captured by two photodiodes (D2, D3). Diode D1 measures the transmitted intensity.

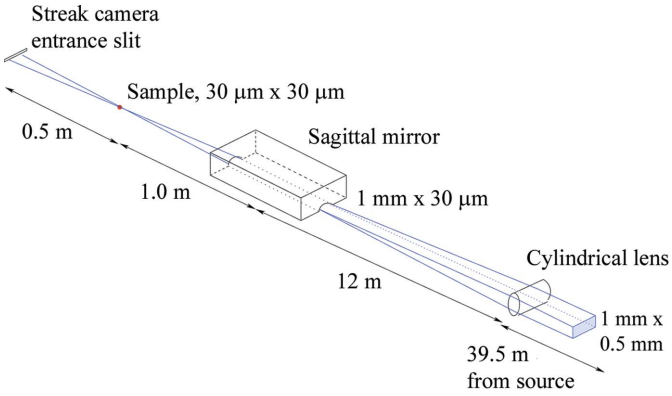

Figure 6
Schematic of the hybrid focusing system.

6. Design details

The hybrid focusing scheme described above is being used to support the X-ray streak camera at the 7-ID beamline of the Advanced Photon Source. For a photon energy of 7.1 keV (the iron *K* absorption edge), a lens with two holes, *i.e.* three bi-concave (BCV) walls, is placed at a point 36 m from the source and 15.5 m to the sample. For 5.5 keV (vanadium *K*-edge), a one-hole (two BCV walls) lens is placed 39.5 m from the source and 12 m to the sample, as shown in Fig. 6.

Both the lens and the mirror are placed inside vacuum vessels that are part of the beam transport piping. The lens is mounted on piezo-driven stages (Newport, 2013) in the following stacking order: rotation about the *y* axis, translation along *x*, rotation about the *u* axis, translation along *v*. The vacuum vessel for the mirror is mounted on a rotation stage (Huber 410), which is sitting on a pair of recirculating-ball-bearing tracks (THK 2RSR15WVMUU+670LM), so that it can be adjusted to the beam, as well as be moved entirely out of the beam path. Inside the vacuum vessel are a goniometer (Thorlabs GNL 10) and a compact vertical lift stage (Melles-Griot TEZ modified to fit a standard micrometer screw). Both stages are driven by motorized micrometer screws (Thorlabs Z612).

7. Operation

A lens placed 39.5 m from the source and 12 m to the sample must have a focal length of $f = 9.20$ m. At a photon energy of 5.5 keV beryllium has $\delta = 1.126 \times 10^{-5}$, and, with holes of $R = 0.5$ mm, equation (2) yields $N = 2.412$, *i.e.* an angle of $\chi = 34^\circ$ for a two-wall lens. Similarly, for a three-wall lens placed 36 m from the source, and 15.5 m to the sample, focusing 7.1 keV X-rays, $N = 3.42$ and the angular setting should be $\chi = 28.6^\circ$.

Figs. 7, 8 and 9 show images of a 5.5 keV X-ray beam at the sample location for different angular settings of the lens. The images were obtained with a CCD camera lens-coupled to a Ce-doped YAG screen. Using a 200 l.p.i. nickel mesh on the YAG screen, the resolution of this imaging system was found to be 0.37 μm per pixel.

All of these images show a weak background of unfocused X-rays due to the higher-harmonic content of the beam. On

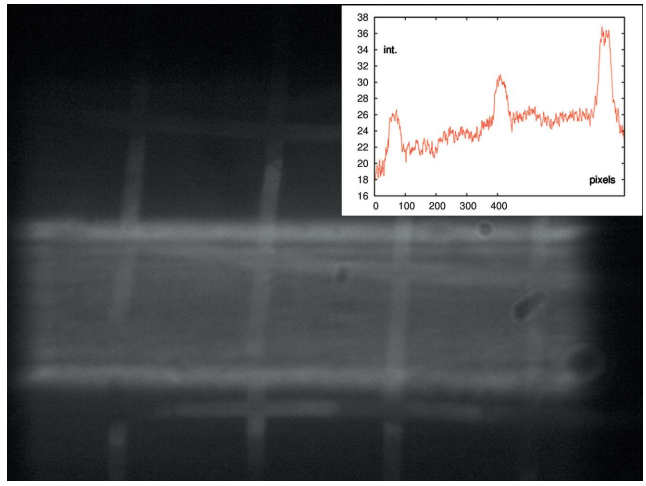

Figure 7
Image of the X-ray beam with the lens at $\chi = 0^\circ$. The grid is due to a nickel mesh with a period of 127 μm placed on the fluorescent screen of the imaging system for calibration purposes. The inset shows a lineout of the grid with 687 pixels/0.254 mm.

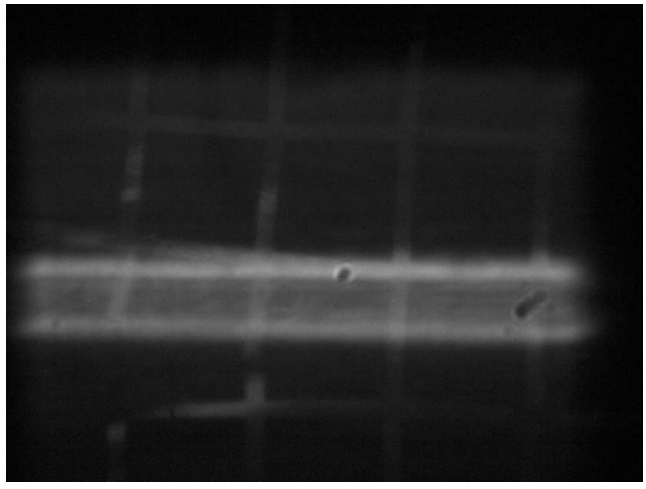

Figure 8
Lens at $\chi = 30^\circ$.

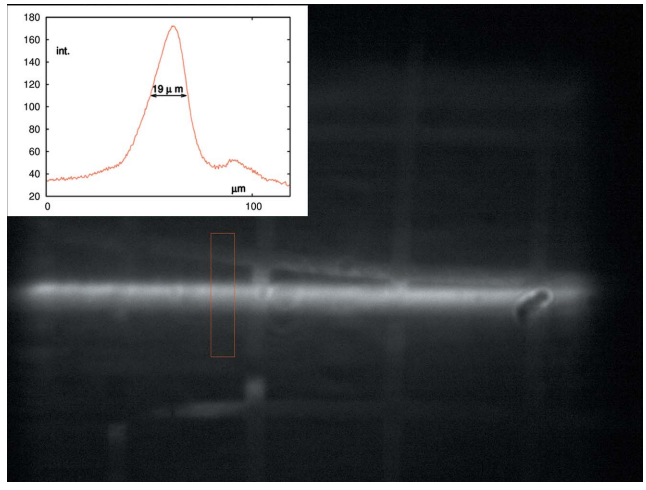

Figure 9
Lens at $\chi = 40^\circ$, best focus. The inset shows a profile through the focus within the indicated box.

top of this is the successively sharper-focused beam of 5.5 keV photons. The images show the optimal focus at $\chi = 40°$. This is in reasonable agreement with the expected value of 34°. The size of 19 μm is considerably larger than the 4 μm one might expect from a 12 μm source (APS, 2013) and a 3:1 demagnification ratio; this is probably due to the cylindrical aberrations of the lens. The discrepancy may be explained with the hole diameter being a little larger than specified, a shift in the source point (subject to the electron optics of the storage ring), or a slight wavefront distortion in the monochromator due to strain on the crystals. Similarly, for the 7.1 keV case, the optimal angle is found at about 45°, and the mismatch with the expected 28.5° may be explained in the same way.

After obtaining an optimal focus with the lens, the mirror is brought in. Figs. 10 to 13 show a sequence of focusing results at different angular settings of the mirror, yielding a spot of 14 μm by 55 μm. The sagittal focus clearly shows the curved ('banana') shape associated with this type of focusing. Unfortunately, this aberration effect degrades the vertical focus to some extent. In the present application, the BPM slit is used to reduce the vertical beam size to 30 μm because the small focal spot matching the laser focus is more important than preservation of the full X-ray flux.

8. Discussion and outlook

The hybrid lens/mirror X-ray focusing scheme presented here is optimized for the requirement of a long focal length in one (vertical) direction and a short focal length in the other. For the long focal length, a mirror would be impractical because of its off-axis deflection of the X-ray beam, and therefore a lens was chosen. For the present application, a relatively inexpensive lens made by drilling holes into beryllium was used. Such a lens introduces circular aberrations, the walls of the holes have some roughness that leads to scattering of radiation, and the walls may be deformed in the process of drilling. All these imperfections were deemed acceptable here but, for

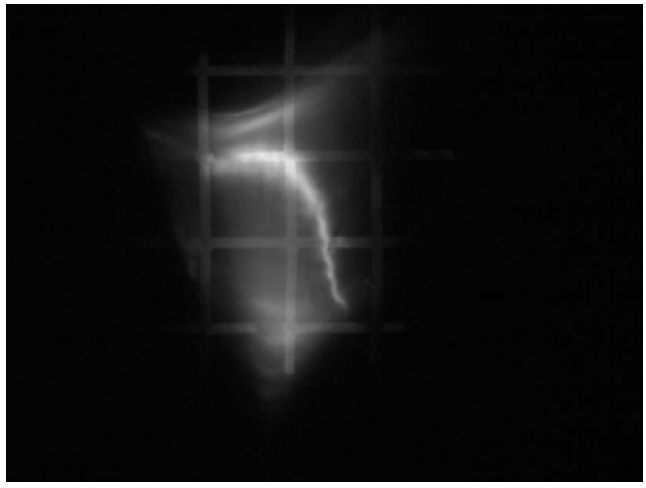

Figure 11
Mirror at 0.2°.

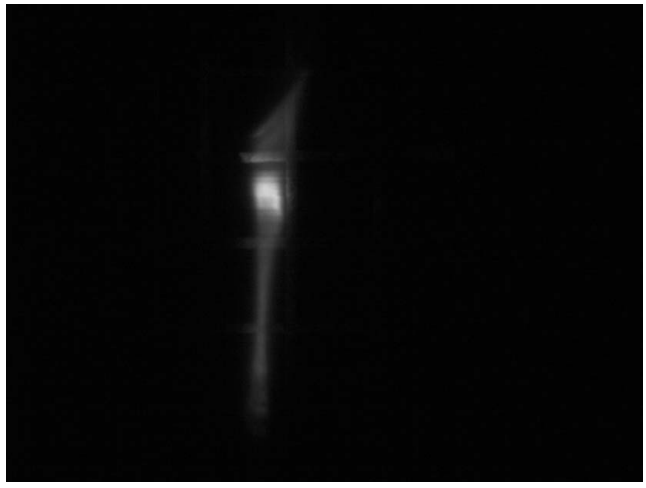

Figure 12
Mirror at 0.225°.

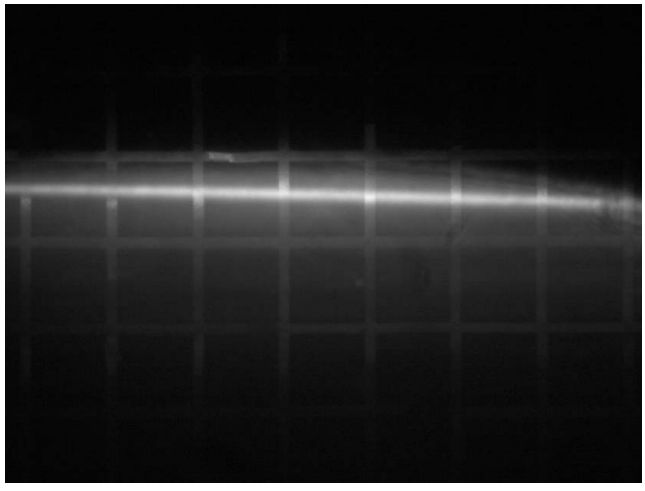

Figure 10
Mirror at 0°. The body of the glass piece with the cylindrical groove is visible as a shadow on the image.

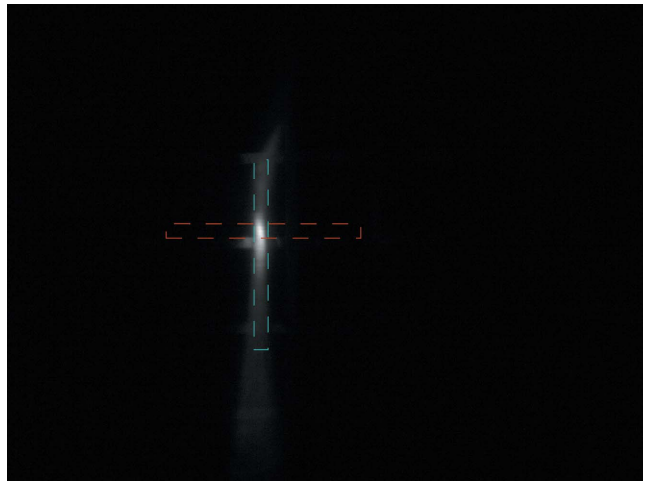

Figure 13
Mirror at 0.23°. The red and blue boxes indicate the regions selected for the profile plots in Fig. 14.

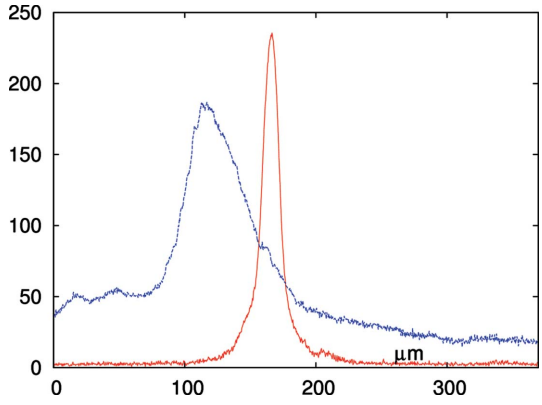

Figure 14
Horizontal and vertical profiles of the focus shown in Fig. 13. The half-widths are 14 μm for the horizontal focus (red) and 55 μm for the vertical (blue).

higher-quality focusing and imaging, a parabolic profile with polished surface should be used for which the method of continuously varying the effective number of holes will work equally well. For the horizontal focus, a lens would be impractical because the short focal length would require a large number of holes (walls between holes) with the associated absorption losses. Therefore, a sagittal mirror was chosen. A sagittal mirror or a lens with many holes (37 holes at 7.1 keV and 1 m focal length) could be chosen, but, overall, a mirror seemed to be a slightly better choice for the present application. Unlike most synchrotron mirrors, this one can be very short because the footprint of the vertically focused X-rays on its surface is only about 13 mm long (for the parameters used here). Focal-length adjustment and dispersion correction of the lens are carried out by a rotation that amounts to a continuous variation of the effective number of holes. The focal length of the sagittal mirror is adjusted through the glancing angle, and no dispersion correction is required.

As a future improvement of this focusing scheme it is planned to include an aberration correction optic to remove the banana shape in the sagittal focus. Furthermore, the stabilizer will be upgraded for multipoint operation to simultaneously maintain the beam pointing and parallelity of the monochromator crystals by acting on the piezo actuator in the monochromator and the vertical position of the lens. The vertical focus could be improved by use of a cylindrical lens with a parabolic profile. A continuous adjustment of the focal length would then leave the parabolic profile intact.

The work at the Advanced Photon Source was supported by the US Department of Energy, Office of Basic Energy Sciences under Contract No. DE-AC02-06CH11357. CRP acknowledges support from the US Department of Energy under grant DE-FG02-08ER15937. We would like to thank M. C. Chollet for his participation in the early stages of this project.

References

Adams, B. W. & Chollet, M. C. (2013). US Patent 8611502.
Ahr, B., Chollet, M., Adams, B., Lunny, E. M., Laperle, C. M. & Rose-Petruck, C. (2011). *Phys. Chem. Chem. Phys.* **13**, 5590–5599.
APS (2013). *Source Point Data*, http://www.aps.anl.gov/Accelerator_Systems_Division/Accelerator_Operations_Physics/SRSource Parameters/sourcePointResults/.
Arms, D., Dufresne, E., Clarke, R., Dierker, S., Pereira, N. & Foster, D. (2002). *Rev. Sci. Instrum.* **73**, 1492–1494.
Chollet, M., Ahr, B., Walko, D., Rose-Petruck, C. & Adams, B. (2011). *IEEE Select Topics Quantum Electron.* **18**, 66–73.
Dufresne, E. M., Adams, B., Arms, D. A., Chollet, M., Landahl, E. C., Li, Y., Walko, D. A. & Wang, J. (2010). *AIP Conf. Proc.* **1234**, 181–184.
Feng, J., Comin, A., Bartelt, A., Shin, H., Nasiatka, J., Padmore, H., Young, A. & Scholl, A. (2007*b*). *Nucl. Instrum. Methods Phys. Res. A*, **582**, 248–251.
Feng, J., Shin, H., Nasiatka, J., Wan, W., Young, A., Huang, G., Comin, A., Byrd, J. & Padmore, H. (2007*a*). *Appl. Phys. Lett.* **91**, 134102.
Insync (2011). *InSync*, http://www.insyncoptics.com.
Khounsary, A. M., Shastri, S. D., Mashayekhi, A., Macrander, A. T., Smither, R. K. & Kraft, F. (2002). *Proc. SPIE*, **4783**, 49–54.
Kohn, V. (2003). *J. Exp. Theo. Phys. (JETP)*, **97**, 204–215.
Krolzig, A., Materlik, G., Swars, M. & Zegenhagen, J. (1984). *Nucl. Instrum. Methods*, **219**, 430–434.
Lengeler, B. (2010). *Refractive X-ray Lenses: New Developments*, http://www.esrf.eu/files/live/sites/www/files/Instrumentation/friday-lectures-slides/B-Lengeler_july2010.pdf.
Lengeler, B., Schroer, C., Tümmler, J., Benner, B., Richwin, M., Snigirev, A., Snigireva, I. & Drakopoulos, M. (1999). *J. Synchrotron Rad.* **6**, 1153–1167.
Liu, J., Wang, J., Shan, B., Wang, C. & Chang, Z. (2003). *Appl. Phys. Lett.* **82**, 3553–3555.
Newport (2013). *Newport Agilis Products*, http://search.newport.com/?i=1;q=Agilis;q1=Product+Series;x1=Resource_Category;content=1.
Ribbing, C., Cederström, B. & Lundquist, M. (2003). *J. Micromech. Microeng.* **13**, 714–720.
Shastri, S. D., Almer, J., Ribbing, C. & Cederström, B. (2007). *J. Synchrotron Rad.* **14**, 204–211.
Vaughan, G. B. M., Wright, J. P., Bytchkov, A., Rossat, M., Gleyzolle, H., Snigireva, I. & Snigirev, A. (2011). *J. Synchrotron Rad.* **18**, 125–133.
Zozulya, A., Bondarenko, S., Schavkan, A., Westermeier, F., Grübel, G. & Sprung, M. (2012). *Opt. Express*, **20**, 18967–18976.